CHEMISTRY OF MATERIALS

pubs.acs.org/cm

Article

Fine Tuning of Defects Enables High Carrier Mobility and Enhanced Thermoelectric Performance of n-Type PbTe

Siqi Wang, Cheng Chang,* Shulin Bai, Bingchao Qin, Yingcai Zhu, Shaoping Zhan, Junqing Zheng, Shuwei Tang, and Li-Dong Zhao*

Cite This: *Chem. Mater.* 2023, 35, 755−763

Read Online

ACCESS | Metrics & More | Article Recommendations | Supporting Information

ABSTRACT: High carrier mobility is critical to improving thermoelectric performance over a broad temperature range. However, traditional doping inevitably deteriorates carrier mobility. Herein, we develop a strategy for fine tuning of defects to improve carrier mobility. To begin, n-type PbTe is created by compensating for the intrinsic Pb vacancy in bare PbTe. Excess Pb^{2+} reduces vacancy scattering, resulting in a high carrier mobility of ∼3400 $cm^2\ V^{-1}\ s^{-1}$. Then, excess Ag is introduced to compensate for the remaining intrinsic Pb vacancies. We find that excess Ag exhibits a dynamic doping process with increasing temperatures, increasing both the carrier concentration and carrier mobility throughout a wide temperature range; specifically, an ultrahigh carrier mobility ∼7300 $cm^2\ V^{-1}\ s^{-1}$ is obtained for $Pb_{1.01}Te$ + 0.002Ag at 300 K. Moreover, the dynamic doping-induced high carrier concentration suppresses the bipolar thermal conductivity at high temperatures. The final step is using iodine to optimize the carrier concentration to ∼10^{19} cm^{-3}. Ultimately, a maximum ZT value of ∼1.5 and a large average ZT_{ave} value of ∼1.0 at 300−773 K are obtained for $Pb_{1.01}Te_{0.998}I_{0.002}$ + 0.002Ag. These findings demonstrate that fine tuning of defects with <0.5% impurities can remarkably enhance carrier mobility and improve thermoelectric performance.

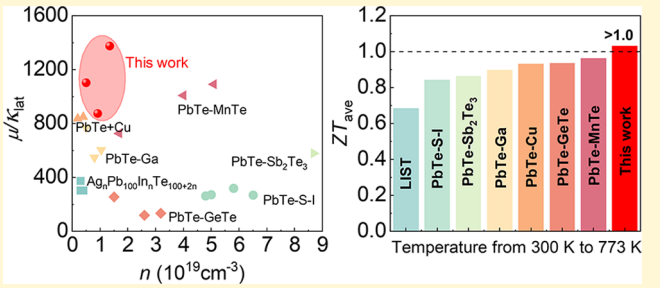

INTRODUCTION

Thermoelectric materials can effectively utilize low-grade heat sources to generate electricity, such as industrial waste heat, automobile exhaust, solar energy, geothermal heat, *etc.*[1−4] To date, the priority of thermoelectric research is to improve the conversion efficiency for more widespread applications. The conversion efficiency depends on the dimensionless figure of merit ZT, $ZT = S^2\sigma T/\kappa$, where S is the Seebeck coefficient, σ is the electrical conductivity, T is the absolute temperature in kelvin, and κ is the total thermal conductivity ($\kappa = \kappa_{lat} + \kappa_{ele} + \kappa_{bi}$, where κ_{lat} is the lattice thermal conductivity, κ_{ele} is the electronic thermal conductivity, κ_{bi} is the bipolar thermal conductivity). In general, thermoelectric enhancement relies heavily on a large Seebeck coefficient, high electrical conductivity, and low thermal conductivity. Nevertheless, the above three thermoelectric parameters are governed primarily by the carrier concentration and are not independently controllable, making them difficult to be optimized simultaneously.[5−9] Researchers have conducted in-depth and fruitful research in upgrading thermoelectric performance *via* combined optimization of electrical and thermal transport. For electrical properties, optimizing carrier concentration,[10−12] increasing carrier mobility,[13,14] and modulating band structure[15−19] are generally applied. For thermal properties, the traditional method is declining the lattice thermal conductivity *via* hierarchical structures, involving atomic-scale defects,[20−22] nanoscale defects,[23−25] and microscale defects.[26,27]

Among a variety of thermoelectric materials, PbTe is a representative thermoelectric material servicing at medium temperature. Numerous research studies have shown that *p*-type PbTe materials have achieved extraordinary thermoelectric properties. Many prominent *p*-type PbTe systems have realized ZT > 2.0, such as $Pb_{0.98}Na_{0.02}Te$,[28] $Pb_{0.98}Na_{0.02}Te$−8% SrTe,[29] $Pb_{0.98}Na_{0.02}Te$−6%MgTe,[30] $Pb_{0.95}Na_{0.05}Te$−0.5% $AgInSe_2$,[31] and $Pb_{0.075}K_{0.025}Te_{0.7}S_{0.3}$.[32] In contrast, their counterpart, n-type PbTe, shows lower ZT values because of the large energy offset (∼0.45 eV) between the conduction bands, so further improvement of n-type PbTe is needed to match p-type PbTe. With time, we discovered several optimization methods that could bring about considerable intensification in the thermoelectric performance of n-type PbTe, such as doping and band engineering.[33] However, even though traditional doping undoubtedly plays a significant role

Received: November 28, 2022
Revised: December 19, 2022
Published: January 9, 2023

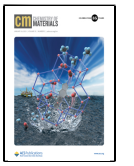

in increasing the carrier concentration, dopants inevitably reduce carrier mobility.[34−36] Band engineering, as another attractive and feasible method, facilitates electrical performance by boosting the effective mass, while it is also detrimental to the carrier mobility.[37,38] In general, these methods are capable of enhancing the maximum ZT, whereas a major drawback is their tendency to decrease carrier mobility, which limits the ZT_{ave}.[39] To ensure good thermoelectric properties over a wide temperature range, comparable n-type PbTe systems with high carrier mobility must be developed.

In this work, fine tuning of defects in PbTe is successively carried out to improve the carrier mobility. First, a small amount of excess Pb (0.004−0.012) is introduced into PbTe. As Pb enters the intrinsic Pb vacancies, n-type PbTe with relatively low carrier concentration is obtained. The dwindling vacancy defects improve carrier mobility, and the maximum carrier mobility reaches ∼3400 $cm^2\ V^{-1}\ s^{-1}$ at 300 K in $Pb_{1.01}Te$. Benefiting from the high carrier mobility, a maximum power factor of ∼31.3 $\mu W\ cm^{-1}\ K^{-2}$ at 300 K is achieved in $Pb_{1.01}Te$. Second, excess Ag is subsequently introduced to fill the remaining Pb vacancies. Results reveal that the comparatively low room-temperature carrier concentration of $\sim 5.5 \times 10^{17}\ cm^{-3}$ leads to a high carrier mobility of ∼7300 $cm^2\ V^{-1}\ s^{-1}$, resulting in a further increased power factor of ∼39.3 $\mu W\ cm^{-1}\ K^{-2}$ at 300 K for $Pb_{1.01}Te$ + 0.002Ag. In particular, Ag atoms in the $Pb_{1.01}Te$ system undergo a dynamic doping process with increasing temperatures, first compensating the Pb vacancies and then entering more interstitial positions due to the temperature-dependent solubility of Ag in the PbTe matrix,[40] which improves the carrier concentration from $\sim 5.5 \times 10^{17}\ cm^{-3}$ at 300 K to $\sim 8.5 \times 10^{18}\ cm^{-3}$ at 873 K for $Pb_{1.01}Te$ + 0.002Ag. Meanwhile, this unique dynamic doping behavior can effectively decouple the carrier concentration and carrier mobility across the entire temperature range and suppress bipolar diffusion at high temperatures. Last, 0.2% of I element (0.002I) is adopted to optimize the carrier concentration while maintaining superior carrier mobility than other n-type PbTe systems with similar carrier concentrations. Meanwhile, the minimum lattice thermal conductivity can reach as low as ∼0.5 $W\ m^{-1}\ K^{-1}$ for $Pb_{1.01}Te_{0.998}I_{0.002}$ + 0.002Ag. As a result, a maximum ZT of ∼1.5 at 773 K and a high average ZT_{ave} of ∼1.0 at 300−773 K are obtained for $Pb_{1.01}Te_{0.998}I_{0.002}$ + 0.002Ag.

EXPERIMENTAL SECTION

All raw materials used in the experiment were simple substances with more than 99.99% purity, including Pb, Te, Ag, and I. First, they were placed in quartz tubes according to the stoichiometric ratio. The quartz tubes were sealed below 10^{-4} Pa and put into a furnace (slowly heating from room temperature to 1323 K for 24 h, holding for 10 h, and finally cooling to room temperature). After the temperature program finished, some silver ingots were obtained, which were then ground into powder for proceeding spark plasma sintering (SPS-211Lx, Dr. Sinter). Finally, the sintered cylindrical, small pieces were cut into rectangles of 10 mm × 3 mm × 3 mm and slices of 8 mm × 8 mm × 1.5 mm to perform electrical and thermal performance tests. The electrical performance was measured by Cryoall CTA (electrical conductivity, σ and Seebeck coefficient, S) and Lake Shore 8400 Series (carrier density, n) instruments. The thermal performance was tested by a Netzsch LFA 457 (thermal diffusivity, D). The thermal conductivity, κ, was estimated by $\kappa = D \times C_p \times \rho$, where C_p is the specific heat capacity based on Debye's law and ρ is the sample density calculated by the ratio of mass to volume. The optical band gap was measured by a Fourier transform infrared spectrometer, IRAffinity-1S, based on the infrared diffuse reflection method.

RESULTS AND DISCUSSION

In this study, the method of fine tuning of defects is used in the PbTe system to achieve superior electrical characteristics while maintaining a relatively low thermal conductivity. Supporting Information to create n-type PbTe, a modest quantity of Pb was first introduced, filling the intrinsic Pb vacancies, which increases carrier mobility and lowers thermal conductivity. Second, excess Ag is adopted for $Pb_{1.01}Te$ to fill the remaining Pb vacancies and also occupy interstitial sites, allowing the $Pb_{1.01}Te + xAg$ system to achieve higher carrier concentration, ultrahigh carrier mobility, and lower thermal conductivity simultaneously across the entire temperature range. Third, the Iodine element is adopted to enhance the carrier concentration, further improving the power factor and restraining the lattice thermal conductivity in the whole temperature range.

Thermoelectric Transport Performance of $Pb_{1+x}Te$. Figure S1a shows the powder X-ray diffraction (XRD) patterns of $Pb_{1+x}Te$ (x = 0, 0.004, 0.006, 0.008, 0.01, 0.012), and the corresponding lattice parameters are given in Figure S1b. All $Pb_{1+x}Te$ samples are NaCl-type cubic structures without extra diffraction peaks detected, and the lattice parameters increase slightly with excess Pb.

As can be seen in Figure 1a, the electrical conductivities decrease first and then increase with increasing Pb amount.

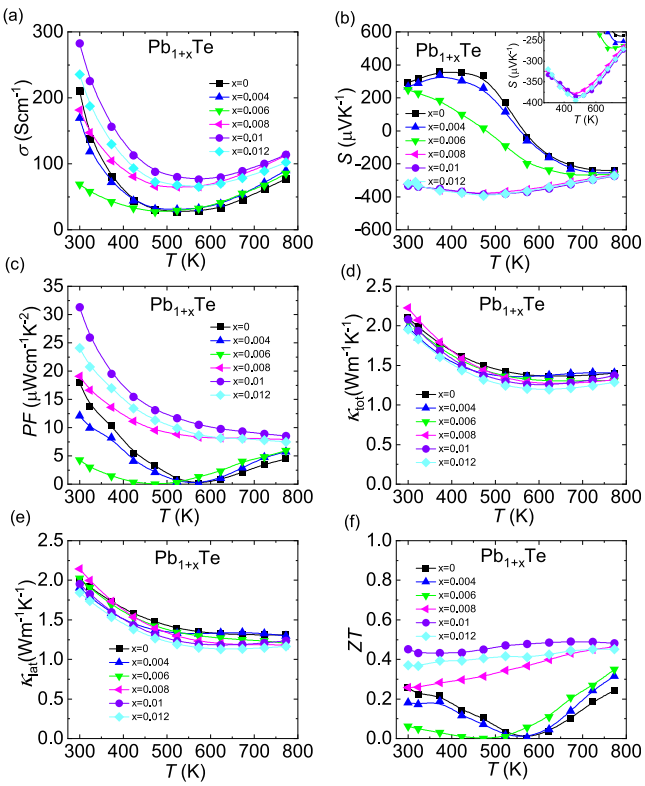

Figure 1. Thermoelectric transport performance of $Pb_{1+x}Te$ (x = 0, 0.004, 0.006, 0.008, 0.01, 0.012): (a) electrical conductivity, (b) Seebeck coefficient, (c) power factor, (d) total thermal conductivity, (e) lattice thermal conductivity, and (f) ZT value.

Correspondingly, $Pb_{1+x}Te$ undergoes a p−n transition at low temperatures, as shown in Figure 1b. Specifically, the Seebeck coefficient of bared PbTe is positive at low temperatures; however, when $x \geq 0.008$, the Seebeck coefficient is completely negative, resulting in n-type PbTe throughout the measuring temperature range. The combined behavior of electrical

https://doi.org/10.1021/acs.chemmater.2c03542
Chem. Mater. 2023, 35, 755−763

conductivity and Seebeck coefficient indicates that the hole concentration in PbTe is suppressed by excess Pb. In Figure 1c, benefitting from the improved electrical conductivity and Seebeck coefficient, the power factor is enhanced significantly, and the maximum value, i.e., room-temperature value, increases notably from ~18.0 μW cm^{-1} K^{-2} for PbTe to ~31.3 μW cm^{-1} K^{-2} for $Pb_{1.01}Te$. In Figure 1d, the total thermal conductivity of PbTe reduces slightly with excess Pb, and the room-temperature value decreases from ~2.1 to ~2.0 Wm^{-1} K^{-1} caused by diminished lattice thermal conductivity, as shown in Figure 1e. $Pb_{1+x}Te$ shows higher electronic thermal conductivity, as shown in Figure S2b, because excess Pb fills the intrinsic Pb vacancies, thereby creating weaker carrier scattering. Ultimately, an average ZT value of ~0.5 for $Pb_{1.01}Te$ is obtained throughout the whole measuring temperature range, as shown in Figure 1f.

To understand the electrical transport evolution of $Pb_{1+x}Te$, we carried out the Hall measurement. In Figure 2a, the carrier concentration of ~10^{17} cm^{-3} in the n-type $Pb_{1+x}Te$ system is relatively low, not as outstanding as the common doping approaches, such as PbTe−Sb[41] (~5.2×10^{19} cm^{-3}), PbTe−I[42] (~1.8×10^{19} cm^{-3}), PbTe−Bi[43] (~2.0×10^{19} cm^{-3}), *etc.*

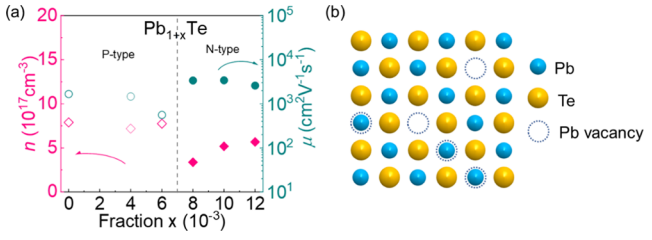

Figure 2. (a) Room-temperature carrier concentration and carrier mobility as a function of Pb and (b) atomic schematic diagram of $Pb_{1+x}Te$.

With the increasing Pb fraction, the carrier concentration is gradually elevated, indicating that more and more Pb enters Pb vacancies. Based on the inverse relationship between carrier concentration and carrier mobility, relatively low carrier concentration brings about high carrier mobility since reduced Pb vacancies alleviate the charge carrier scattering, and the maximum carrier mobility can reach ~3400 cm^2 V^{-1} s^{-1} for $Pb_{1.01}Te$. Figure 2b shows the atomic schematic diagram of the $Pb_{1+x}Te$ system, graphically depicting the phenomenon that excess Pb atoms occupy the intrinsic Pb vacancies.

Electrical Transport Performance of $Pb_{1.01}Te$ + *x*Ag. The powder X-ray diffraction (XRD) measurements of $Pb_{1.01}Te$ + xAg (x = 0−0.005) samples are performed, as shown in Figure S4a. All samples are NaCl cubic structures, and no peaks of impurities are found. Likewise, the small amount of excess Ag results in a slight expansion of the lattice parameters, as shown in Figure S4b.

Figure 3 shows that excess Ag significantly improves the electrical transport performance of the $Pb_{1.01}Te$ + xAg system. Figure 3a shows a clear increase in electrical conductivity throughout the whole temperature range. In particular, the electrical conductivity increases anomaly above 500 K. In Figure 3b, the negative Seebeck coefficients prove that $Pb_{1.01}Te$ + xAg is electron-dominated n-type material. The introduction of Ag reduces the Seebeck coefficient, and the maximum absolute value decreases from ~385.9 μV K^{-1} for $Pb_{1.01}Te$ to ~249.0 μV K^{-1} for $Pb_{1.01}Te$ + 0.002Ag. The Pisarenko curve in Figure S5 reveals that the effective mass of the $Pb_{1.01}Te$ + xAg system remains approximately 0.22m_0, indicating that the depressed Seebeck coefficient of $Pb_{1.01}Te$ + xAg is attributed to the elevated carrier concentration rather than the reduced effective mass. As a result, significantly incremental electrical conductivity and abated Seebeck coefficient further enhance the power factor compared to $Pb_{1.01}Te$. In particular, a superior room-temperature power factor of ~39.3 μW cm^{-1} K^{-2} is

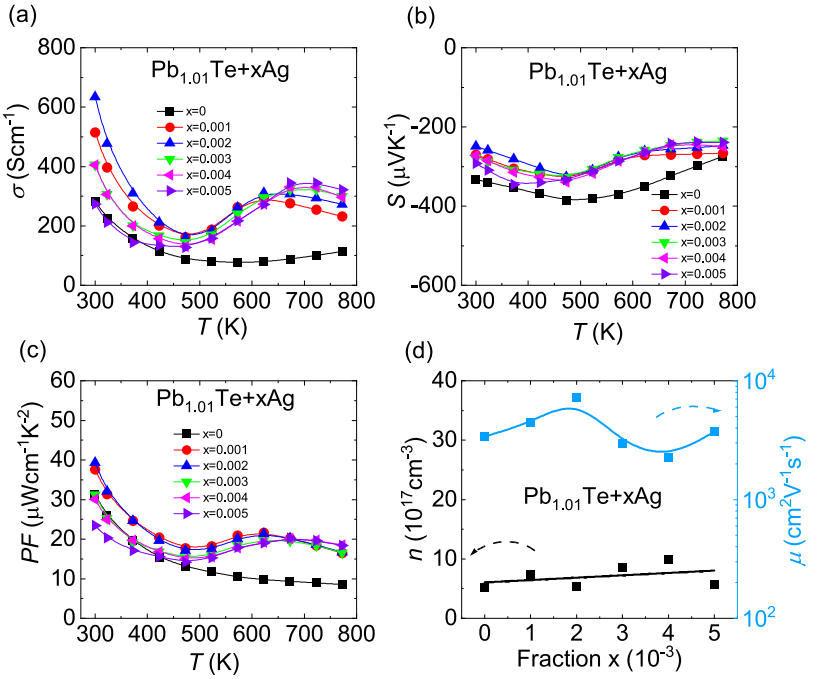

Figure 3. Electrical transport performance of $Pb_{1.01}Te$ + xAg (x = 0−0.005): (a) electrical conductivity, (b) Seebeck coefficient, (c) power factor, and (d) room-temperature carrier concentration and carrier mobility as a function of Ag.

https://doi.org/10.1021/acs.chemmater.2c03542
Chem. Mater. 2023, 35, 755−763

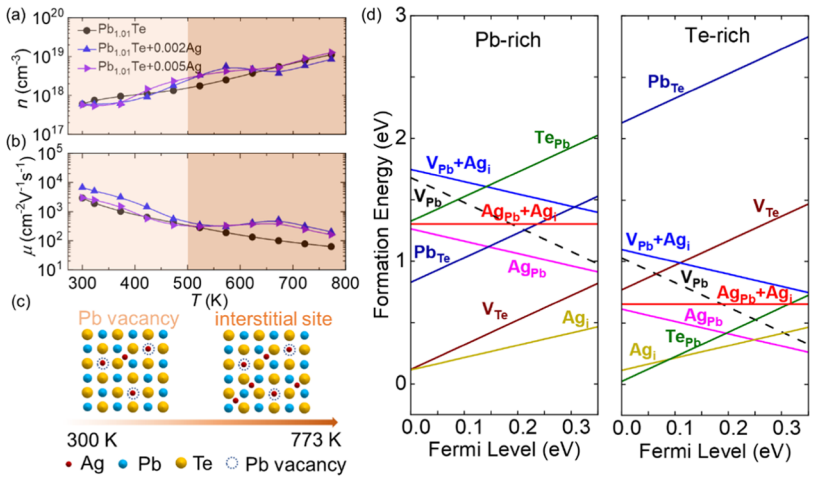

Figure 4. Dynamic doping process in $Pb_{1.01}Te$ + *x*Ag: (a) carrier concentration and (b) carrier mobility as a function of temperature, (c) atomic schematic diagram, and (d) calculated defect formation energies of PbTe.

acquired for $Pb_{1.01}Te$ + 0.002Ag, as shown in Figure 3c. Also, the power factor above 500 K is twice higher as that of $Pb_{1.01}Te$. Figure 3d shows the carrier concentration and carrier mobility of $Pb_{1.01}Te$ + *x*Ag at room temperature. Carrier concentration increases as the Ag fraction rises; however, carrier mobility is not impaired. Particularly, the maximum carrier mobility is increased by more than twice from ~3400 $cm^2\ V^{-1}\ s^{-1}$ for $Pb_{1.01}Te$ to ~7300 $cm^2\ V^{-1}\ s^{-1}$ for $Pb_{1.01}Te$ + 0.002Ag.

To get an insight into the remarkable electrical transport properties of $Pb_{1.01}Te$ + *x*Ag, we measured the temperature-dependent carrier concentration, as shown in Figure 4a,b. The carrier concentrations of bare PbTe and $Pb_{1.01}Te$ increase with increasing temperatures, as shown in Figure S6, which is derived from the low carrier concentration and thus pronounced bipolar effect at high temperatures.[44] However, $Pb_{1.01}Te$ + *x*Ag systems still exhibit increasing carrier concentration throughout the temperature range even though their bipolar effect is suppressed (the suppressed bipolar effect is evidenced by the low bipolar thermal conductivity, which is discussed in detail in the next section). We attribute the abnormal temperature-dependent behavior of carrier concentration to Ag-induced dynamic doping.[40] The dynamic doping process in $Pb_{1.01}Te$ + *x*Ag is initiated by the multiple occupancies of Ag atoms with increasing temperatures, and Figure 4c displays the phenomena in detail. At 300−500 K, Ag atoms compensate for intrinsic Pb vacancies and interstitials, enhancing carrier mobility, as shown in Figure 4b. Above 500 K, more Ag atoms occupy interstitial positions to provide excess electrons for the system, resulting in a higher carrier concentration than the $Pb_{1.01}Te$ sample. It is noteworthy that the carrier mobilities of $Pb_{1.01}Te$ + Ag at high temperatures are also higher than those of $Pb_{1.01}Te$, which can be explained by the suppressed bipolar effect. As a result, the carrier mobility of $Pb_{1.01}Te$ + Ag is greater than that of $Pb_{1.01}Te$ in the entire temperature range.

To further reveal the role of Ag in PbTe, we utilized first principles to calculate various defects and their formation energy in the system, such as vacancies, interstitials, antisites, and Ag-filled intrinsic vacancies. Figure 4d depicts the calculated formation energy of related defects. Based on the existence of Pb vacancies, the formation energy of Pb vacancies in the Pb-rich system is greater than that in the Te-rich system, implying that Pb vacancies are more difficult to form in the Pb-rich condition. For $Pb_{1.01}Te$ (Pb-rich system), the formation energy of Ag_{Pb} (Ag-occupied Pb vacancies) is lower than that of V_{Pb} (Pb vacancies), indicating that the introduction of Ag reduces the Pb vacancies, thereby lowering the content of point defects and improving the carrier mobility. The formation energy of Ag_i (Ag interstitials) is also very low in both Pb-rich and Te-rich systems, demonstrating that Ag not only fills Pb vacancies but also occupies the interstitials in PbTe. The calculated results of defect formation energy well support the experimental results and verify the role of the Ag element in improving the electrical transport performance of the $Pb_{1.01}Te$ system.

Thermal Transport Performance of $Pb_{1.01}Te$ + *x*Ag. Figure 5 displays the temperature-dependent thermal properties of $Pb_{1.01}Te$ + *x*Ag. In Figure 5a, the total thermal conductivity decreases slightly. The electronic thermal conductivity is calculated from equation $\kappa_{ele} = L\sigma T$ (L is the Lorenz number, as shown in Figure S7a, determined by the single parabolic band (SPB) model). Because of the greater electrical conductivity, the $Pb_{1.01}Te$ + *x*Ag system displays much higher electronic thermal conductivity than $Pb_{1.01}Te$, as shown in Figure 5b. Figure 5c presents the lattice thermal conductivity κ_{lat} calculated by $\kappa_{lat} = \kappa_{tot} - \kappa_{ele}$ as a function of temperature. In the high-temperature region, all of the $Pb_{1.01}Te$ + *x*Ag samples exhibit lower κ_{lat} than $Pb_{1.01}Te$ since the elevated electronic thermal conductivity of $Pb_{1.01}Te$ + *x*Ag effectively suppresses the bipolar diffusion. Excess Ag depresses the minimum lattice thermal conductivity from ~1.2 $Wm^{-1}\ K^{-1}$ for $Pb_{1.01}Te$ to ~0.7 $Wm^{-1}\ K^{-1}$ for $Pb_{1.01}Te$ + 0.005Ag. The solid black line in Figure 5c is the theoretical lattice thermal conductivity of PbTe without bipolar thermal conductivity. The theoretical lattice thermal conductivity as a function of the temperature follows the relationship[30]

$$\kappa_{lat} = 3.5\left(\frac{k_B}{\hbar}\right)^3 \frac{MV^{1/3}\theta_D^3}{\gamma^2 T}$$

where k_B is the Boltzmann constant, $\hbar$ is the Planck constant, M is the average atomic mass, V is the average atomic volume, θ_D is the Debye temperature, and γ is the Gruneisen constant. The $\kappa_{tot} - \kappa_{ele}$ values of $Pb_{1.01}Te$ + *x*Ag samples coincide with the calculated values, indicating that the bipolar diffusion is

https://doi.org/10.1021/acs.chemmater.2c03542
Chem. Mater. 2023, 35, 755−763

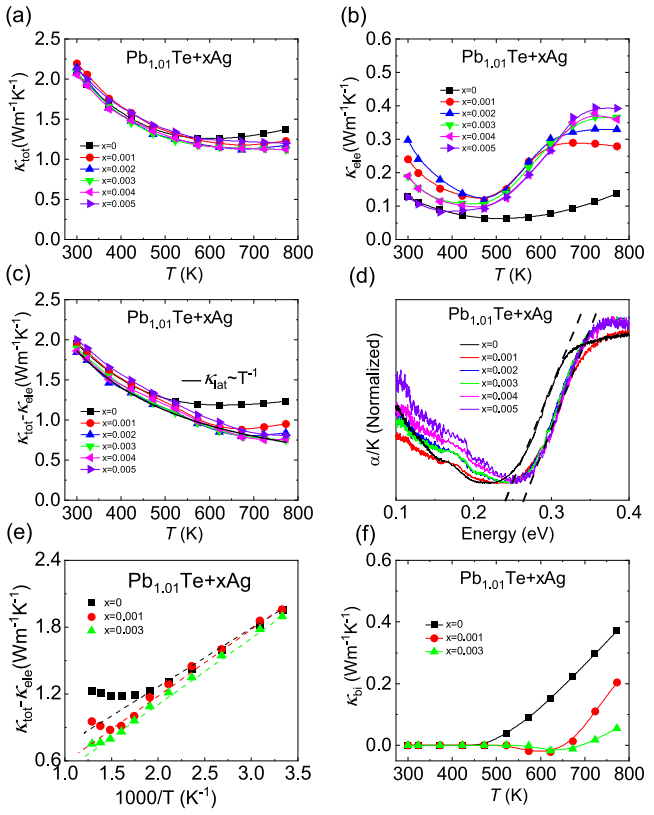

Figure 5. Thermal transport performance of $Pb_{1.01}Te + xAg$ (x = 0–0.005): (a) total thermal conductivity, (b) electronic thermal conductivity, (c) $\kappa_{tot} - \kappa_{ele}$ as a function of T, (d) room-temperature band gap, (e) $\kappa_{tot} - \kappa_{ele}$ as a function of $1000/T$, and (f) bipolar thermal conductivity.

suppressed in $Pb_{1.01}Te + xAg$. Meanwhile, the enlarged band gap is responsible for restrained bipolar diffusion due to the following formula[45,46]

$$\kappa_{bi} = A \exp\left(\frac{-E_g}{2k_B T}\right)$$

where A is the constant and E_g is the band gap. Ag enlarges the band gap in Figure 5d, thereby reducing the bipolar thermal conductivity. The $(\kappa_{tot} - \kappa_{ele}) - 1000\ T^{-1}$ relationship is plotted in Figure 5e to examine the contribution of bipolar thermal conductivity, revealing that the true lattice thermal conductivity should be a straight line, while the $\kappa_{tot} - \kappa_{ele}$ values in the high-temperature region are higher than the predicted values, indicating that bipolar diffusion occurs in this region. According to Figure 5f, bipolar thermal conductivity is the difference between the solid line and the dotted line and decreases as the amount of Ag increases.

***ZT* Values of $Pb_{1.01}Te + xAg$.** Comparing room-temperature carrier mobility of the $Pb_{1.01}Te + xAg$ system with those of the other n-type PbTe materials, we found that this system exhibits superior carrier mobility of ~7300 $cm^2\ V^{-1}\ s^{-1}$ at low carrier concentrations (~10^{17} cm^{-3}), as shown in Figure 6a, which is competitive in high-performance n-type PbTe-based materials. Finally, as a result of ultrahigh carrier mobility and suppressed bipolar thermal conductivity, room-temperature ZT, as shown in Figure 6b, is further enhanced from ~0.5 for $Pb_{1.01}Te$ to ~0.6 for $Pb_{1.01}Te + 0.002Ag$, and high-temperature

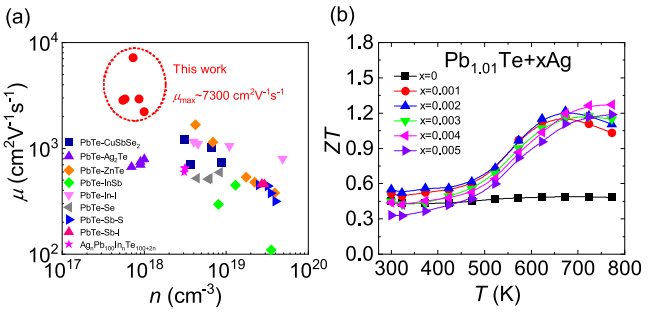

Figure 6. (a) Comparison of carrier mobility as a function of the carrier concentration of n-type PbTe and (b) ZT values of $Pb_{1.01}Te + xAg$.

ZT is significantly increased from ~0.5 for $Pb_{1.01}Te$ to ~1.3 for $Pb_{1.01}Te + 0.004Ag$.

Thermoelectric Transport Performance of $Pb_{1.01}Te_{1-x}I_x$ + 0.002Ag. Based on $Pb_{1.01}Te + 0.002Ag$ with the maximum average ZT, I doping is employed to increase the carrier concentration, thereby improving the electrical performance. Figure S8 shows the phase identification of $Pb_{1.01}Te_{1-x}I_x + 0.002Ag$ (x = 0–0.003). No new peak is found in Figure S8a, and the samples still denote the NaCl structure. The lattice parameter decreases slightly in $Pb_{1.01}Te_{1-x}I_x + 0.002Ag$, as shown in Figure S8b, because smaller I^- (~2.06 Å) substitutes for larger Te^{2-} (~2.11 Å). Figure 7 depicts the thermoelectric performance of $Pb_{1.01}Te_{1-x}I_x + 0.002Ag$ (x = 0–0.003). I doping can effectively improve the electrical conductivity, as shown in

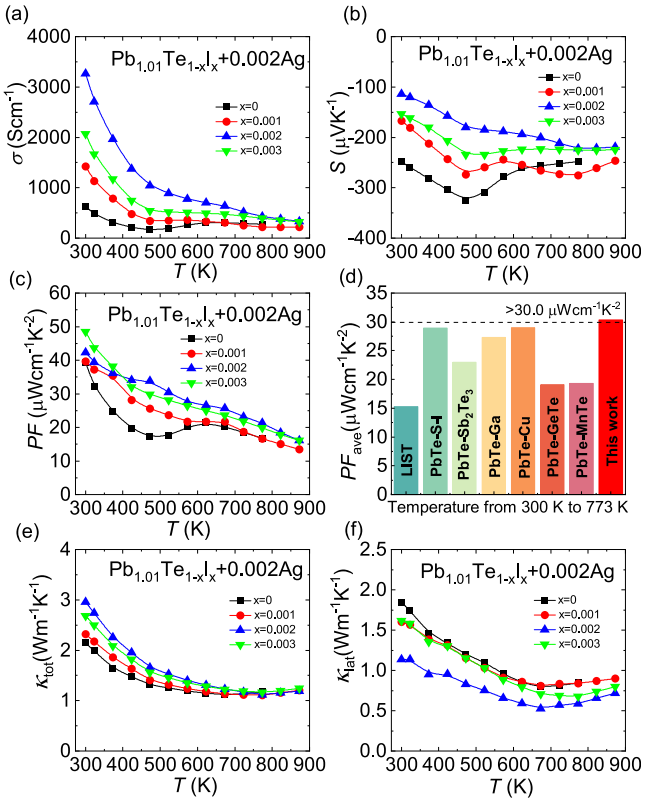

Figure 7. Thermoelectric transport performance of $Pb_{1.01}Te_{1-x}I_x + 0.002Ag$ (x = 0–0.003): (a) electrical conductivity, (b) Seebeck coefficient, (c) power factor, (d) average power factor, (e) total thermal conductivity, and (f) lattice thermal conductivity.

https://doi.org/10.1021/acs.chemmater.2c03542
Chem. Mater. 2023, 35, 755–763

Figure 7a. The room-temperature electrical conductivity can be magnified from ~633.5 S cm^{-1} for $Pb_{1.01}Te$ + 0.002Ag to ~3267.8 S cm^{-1} for $Pb_{1.01}Te_{0.998}I_{0.002}$ + 0.002Ag. The Seebeck coefficients of all samples in Figure 7b are negative, showing n-type semiconductor characteristics. The absolute value of the Seebeck coefficient of $Pb_{1.01}Te_{1-x}I_x$ + 0.002Ag decreases with increasing doping amount of the I element since the more I content, the higher the carrier concentration, as shown in Figure S9. The high electrical conductivity and low Seebeck coefficient of the $Pb_{1.01}Te_{1-x}I_x$ + 0.002Ag system indicate that the I element possesses extremely high doping efficiency in PbTe. The carrier concentration can be efficiently increased by doping with as little as 0.002I. Figure 7c shows that the power factor increases across the entire temperature range, with the maximum power factor increasing from ~39.3 μW cm^{-1} K^{-2} for $Pb_{1.01}Te$ + 0.002Ag to ~48.5 μW cm^{-1} K^{-2} for $Pb_{1.01}Te_{0.998}I_{0.002}$ + 0.002Ag. The average power factor exceeds ~30.0 μW cm^{-1} K^{-2} for $Pb_{1.01}Te_{0.998}I_{0.002}$ + 0.002Ag, which is higher than those of other n-type PbTe systems (PbTe−S−I,[47] PbTe−Sb_2Te_3−Sb−Cu_2Te,[23] $Ag_nPb_{100}InTe_{100+2n}$,[48] PbTe + Cu,[49] PbTe−GeTe,[50] PbTe−MnTe,[51] PbTe−Ga[52]), as shown in Figure 7d. In Figure 7e, the total thermal conductivity of $Pb_{1.01}Te_{1-x}I_x$ + 0.002Ag increases with increasing I content, primarily owing to an enhancement in electronic thermal conductivity. The lattice thermal conductivity decreases with increasing I content, as shown in Figure 7f, due to the enhanced phonon scattering. The minimum lattice thermal conductivity is reduced to ~0.5 Wm^{-1} K^{-1} for $Pb_{1.01}Te_{0.998}I_{0.002}$ + 0.002Ag.

To comprehensively evaluate the thermoelectric performance of the $Pb_{1.01}Te_{1-x}I_x$ + 0.002Ag system, the relationship between carrier concentration and the ratio of carrier mobility to lattice thermal conductivity (μ/κ_{lat}) is plotted, as shown in Figure 8a. Compared with other high-performance n-type PbTe systems (PbTe−S−I,[47] PbTe−Sb_2Te_3−Sb−Cu_2Te,[23] $Ag_nPb_{100}InTe_{100+2n}$,[48] PbTe + Cu,[49] PbTe−GeTe,[50] PbTe−MnTe,[51] PbTe−Ga[52]), the $Pb_{1.01}Te_{1-x}I_x$ + 0.002Ag system possesses higher μ/κ_{lat} values at lower carrier concentrations, indicating that a trace of Pb atoms (Pb-occupied Pb vacancies) and Ag atoms (Ag-occupied Pb vacancies) can effectively regulate the intrinsic defects in PbTe and reduce the scattering for charge carriers, protecting the charge carrier transport while scattering phonon. Accordingly, owing to a better balance between electrons and phonons, the ZT value increases in the whole temperature range, and the maximum ZT value is enhanced from ~1.2 for $Pb_{1.01}Te$ + 0.002Ag to ~1.5 for $Pb_{1.01}Te_{0.998}I_{0.002}$ + 0.002Ag, as shown in Figure 8b. Figure 8c,d shows the comparison of ZT values and average ZT_{ave} values with various n-type PbTe materials, respectively. The large ZT values of $Pb_{1.01}Te_{0.998}I_{0.002}$ + 0.002Ag in the whole temperature zone contribute to the excellent average ZT_{ave} value, reaching >1.0 at 300−773 K.

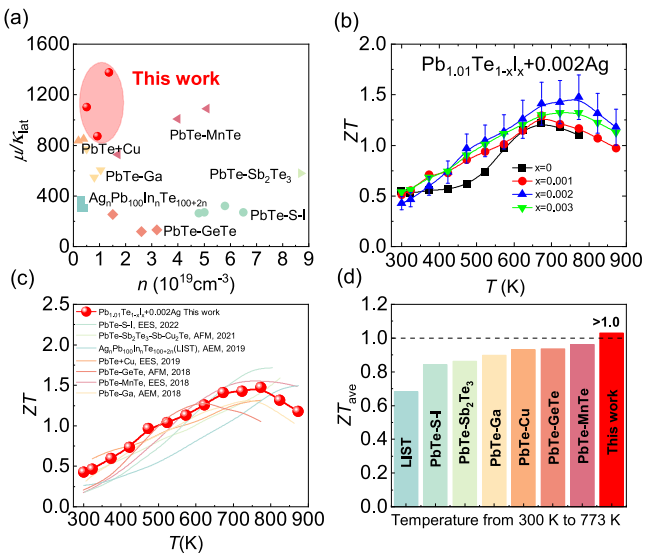

Figure 8. Comparisons of thermoelectric parameters of $Pb_{1.01}Te_{1-x}I_x$ + 0.002Ag with those of other systems: (a) diagram of μ/κ_{lat} and (b) ZT values of $Pb_{1.01}Te_{1-x}I_x$ + 0.002Ag. Comparisons of (c) ZT values and (d) average ZT values of $Pb_{1.01}Te_{0.998}I_{0.002}$ + 0.002Ag with those of other PbTe systems.

CONCLUSIONS

This work has provided a deeper insight into designing fine-tuned defects to improve the carrier mobility of n-type PbTe. In particular, by introducing a small amount of Pb, the reduced Pb vacancy improves the carrier mobility to ~3400 cm^2 V^{-1} s^{-1} at 300 K for $Pb_{1.01}Te$. Then, the room-temperature carrier mobility can reach as high as ~7300 cm^2 V^{-1} s^{-1} for $Pb_{1.01}Te$ + 0.002Ag due to Ag-induced dynamic doping. Finally, Iodine doping dramatically increases the carrier concentration while maintaining superior carrier mobility compared to other PbTe systems with only traditional dopants. The combination of high carrier mobility and the suppressed bipolar effect enables the significant enhancement of thermoelectric performance with a high ZT ~1.5 at 773 K and average ZT_{ave} ~1.0 at 300−773 K for n-type $Pb_{1.01}Te_{0.998}I_{0.002}$ + 0.002Ag. These findings provide insights into balancing electron and phonon transport *via* fine tuning of defects, which could be a promising aspect of co-optimizing thermal and electrical performance of materials with instinct defects.

ASSOCIATED CONTENT

Supporting Information

The Supporting Information is available free of charge at https://pubs.acs.org/doi/10.1021/acs.chemmater.2c03542.

Density functional theory (DFT) calculations, formula of the average PF_{ave} value, phase identification of $Pb_{1+x}Te$ (x = 0, 0.004, 0.006, 0.008, 0.01, 0.0012) (Figure S1), thermoelectric transport properties as a function of temperature for $Pb_{1+x}Te$ (x = 0, 0.004, 0.006, 0.008, 0.01, 0.0012) (Figure S2), sample density of $Pb_{1+x}Te$ (x = 0, 0.004, 0.006, 0.008, 0.01, 0.0012) (Figure S3); phase identification of $Pb_{1.01}Te$ + xAg (x = 0−0.005) (Figure S4), room-temperature Pisarenko plots of $Pb_{1.01}Te$ + xAg (Figure S5), carrier concentration of PbTe and $Pb_{1.01}Te$ as a function of temperature (Figure S6), thermoelectric transport properties as a function of temperature for $Pb_{1.01}Te$ + xAg (x = 0−0.005) (Figure S7), phase identification of $Pb_{1.01}Te_{1-x}I_x$ + 0.002Ag (x = 0−0.003) (Figure S8), room-temperature carrier density and carrier mobility as a function of Ag doping content (Figure S9), thermoelectric transport properties as a function of temperature for $Pb_{1.01}Te_{1-x}I_x$ + 0.002Ag (x = 0−0.003) (Figure S10), and sample density of $Pb_{1.01}Te_{1-x}I_x$ + 0.002Ag (x = 0−0.003) (Figure S11) (PDF)

https://doi.org/10.1021/acs.chemmater.2c03542
Chem. Mater. 2023, 35, 755−763

AUTHOR INFORMATION

Corresponding Authors

Cheng Chang − *Institute of Science and Technology Austria, 3400 Klosterneuburg, Austria;* orcid.org/0000-0002-9515-4277; Email: cheng.chang@ist.ac.at

Li-Dong Zhao − *School of Materials Science and Engineering, Beihang University, Beijing 100191, China;* orcid.org/0000-0003-1247-4345; Email: zhaolidong@buaa.edu.cn

Authors

Siqi Wang − *School of Materials Science and Engineering, Beihang University, Beijing 100191, China*

Shulin Bai − *School of Materials Science and Engineering, Liaoning Technical University, Fuxin 123000, China*

Bingchao Qin − *School of Materials Science and Engineering, Beihang University, Beijing 100191, China;* orcid.org/0000-0003-2720-5922

Yingcai Zhu − *School of Materials Science and Engineering, Beihang University, Beijing 100191, China*

Shaoping Zhan − *School of Materials Science and Engineering, Beihang University, Beijing 100191, China*

Junqing Zheng − *School of Materials Science and Engineering, Beihang University, Beijing 100191, China*

Shuwei Tang − *School of Materials Science and Engineering, Liaoning Technical University, Fuxin 123000, China;* orcid.org/0000-0002-3963-8031

Complete contact information is available at: https://pubs.acs.org/10.1021/acs.chemmater.2c03542

Author Contributions

The manuscript was written through the contribution of all authors. All authors have given approval for the final version of the manuscript. Siqi Wang, research design, data collection and analysis, and draft writing and editing; Shulin Bai and Shuwei Tang, density functional theory (DFT) calculations; Bingchao Qin, Yingcai Zhu, Shaoping Zhan, and Junqing Zheng, data analysis; Cheng Chang and Li-Dong Zhao, research design, data analysis, draft writing and editing, and funding acquisition.

Funding

The National Key Research and Development Program of China (2018YFA0702100), the Basic Science Center Project of the National Natural Science Foundation of China (51788104), the National Natural Science Foundation of China (51571007 and 51772012), the Beijing Natural Science Foundation (JQ18004), the 111 Project (B17002), the National Science Fund for Distinguished Young Scholars (51925101), and the FWF "Lise Meitner Fellowship" (grant agreement M2889-N). Open Access is funded by the Austrian Science Fund (FWF).

Notes

The authors declare no competing financial interest.

ACKNOWLEDGMENTS

This work was supported by the National Key Research and Development Program of China (2018YFA0702100), the Basic Science Center Project of the National Natural Science Foundation of China (51788104), the National Natural Science Foundation of China (51571007 and 51772012), the Beijing Natural Science Foundation (JQ18004), the 111 Project (B17002), and the National Science Fund for Distinguished Young Scholars (51925101). C.C. acknowledges funding from the FWF "Lise Meitner Fellowship" (grant agreement M2889-N).

REFERENCES

(1) Su, L. Z.; Wang, D. Y.; Wang, S. N.; Qin, B. C.; Wang, Y. P.; Qin, Y. X.; Jin, Y.; Chang, C.; Zhao, L. D. High Thermoelectric Performance Realized through Manipulating Layered Phonon-Electron Decoupling. *Science* **2022**, *375*, 1385−1389.

(2) Hu, C. L.; Xia, K. Y.; Fu, C. G.; Zhao, X. B.; Zhu, T. J. Carrier Grain Boundary Scattering in Thermoelectric Materials. *Energy Environ. Sci.* **2022**, *15*, 1406−1422.

(3) Bu, Z. L.; Zhang, X. Y.; Hu, Y. X.; Chen, Z. W.; Lin, S. Q.; Li, W.; Xiao, C.; Pei, Y. Z.; Record, A. Thermoelectric Efficiency in Tellurium-Free Modules for Low-Grade Waste Heat Recovery. *Nat. Commun.* **2022**, *13*, No. 237.

(4) Chang, C.; Kanatzidis, M. G. High-Entropy Thermoelectric Materials Emerging. *Mater. Lab* **2022**, *1*, No. 220048.

(5) Shi, X. L.; Zou, J.; Chen, Z. G. Advanced Thermoelectric Design: From Materials and Structures to Devices. *Chem. Rev.* **2020**, *120*, 7399−7515.

(6) Zhou, C. J.; Lee, Y. K.; Yu, Y.; Byun, S.; Luo, Z. Z.; Lee, H.; Ge, B. Z.; Lee, Y. L.; Chen, X. Q.; Lee, J. Y.; Cojocaru-Miredin, O.; Chang, H.; Im, J.; Cho, S. P.; Wuttig, M.; Dravid, V. P.; Kanatzidis, M. G.; Chung, I. Polycrystalline SnSe with a Thermoelectric Figure of Merit Greater Than the Single Crystal. *Nat. Mater.* **2021**, *20*, 1378−1385.

(7) Zheng, Y.; Slade, T. J.; Hu, L.; Tan, X. Y.; Luo, Y. B.; Luo, Z. Z.; Xu, J. W.; Yan, Q. Y.; Kanatzidis, M. G. Defect Engineering in Thermoelectric Materials: What Have We Learned? *Chem. Soc. Rev.* **2021**, *50*, 9022−9054.

(8) Liu, W. S.; Yan, X.; Chen, G.; Ren, Z. F. Recent Advances in Thermoelectric Nanocomposites. *Nano Energy* **2012**, *1*, 42−56.

(9) Qin, B. C.; Zhao, L. D. Carriers: the Less, the Faster. *Mater. Lab* **2022**, *1*, No. 220004.

(10) Luo, Z. Z.; Cai, S. T.; Hao, S. Q.; Bailey, T. P.; Luo, Y. B.; Luo, W. J.; Yu, Y.; Uher, C.; Wolverton, C.; Dravid, V. P.; Zou, Z. G.; Yan, Q. Y.; Kanatzidis, M. G. Extraordinary Role of Zn in Enhancing Thermoelectric Performance of Ga-doped n-type PbTe. *Energy Environ. Sci.* **2022**, *15*, 368−375.

(11) Xing, T.; Zhu, C. X.; Song, Q. F.; Huang, H.; Xiao, J.; Ren, D. D.; Shi, M. J.; Qiu, P. F.; Shi, X.; Xu, F. F.; Chen, L. D. Ultralow Lattice Thermal Conductivity and Superhigh Thermoelectric Figure-of-Merit in (Mg, Bi) Co-Doped GeTe. *Adv. Mater.* **2021**, *33*, No. 2008773.

(12) Cui, J.; Wang, M. M.; Xu, X.; Chen, Y.; He, J. Q. Understanding the Effects of Iodine Doping on the Thermoelectric Performance of n-type PbTe Ingot Materials. *J. Appl. Phys.* **2019**, *126*, No. 025108.

(13) Xiao, Y.; Xu, L. Q.; Hong, T.; Shi, H. N.; Wang, S. N.; Gao, X.; Ding, X. D.; Sun, J.; Zhao, L. D. Ultrahigh Carrier Mobility Contributes to Remarkably Enhanced Thermoelectric Performance in n-type PbSe. *Energy Environ. Sci.* **2021**, *15*, 246−355.

(14) Cohen, I.; Kaller, M.; Komisarchik, G.; Fuks, D.; Gelbstein, Y. Enhancement of the Thermoelectric Properties of n-type PbTe by Na and Cl Co-Doping. *J. Mater. Chem. C* **2015**, *3*, 9559−9564.

(15) Dutta, M.; Biswas, R. K.; Pati, S. K.; Biswas, K. Discordant Gd and Electronic Band Flattening Synergistically Induce High Thermoelectric Performance in n-type PbTe. *ACS Energy Lett.* **2021**, *6*, 1625−1632.

(16) Xie, G. Z.; Li, Z.; Luo, T. T.; Bai, H.; Sun, J. C.; Xiao, Y.; Zhao, L. D.; Wu, J. S.; Tan, G. J.; Tang, X. F. Band Inversion Induced Multiple Electronic Valleys for High Thermoelectric Performance of SnTe with Strong Lattice Softening. *Nano Energy* **2020**, *69*, No. 104395.

(17) Xiao, Y.; Wang, D. Y.; Zhang, Y.; Chen, C. R.; Zhang, S. X.; Wang, K. D.; Wang, G. T.; Pennycook, S. J.; Snyder, G. J.; Wu, H. J.; Zhao, L. D. Band Sharpening and Band Alignment Enable High Quality Factor to Enhance Thermoelectric Performance in n-type PbS. *J. Am. Chem. Soc.* **2020**, *142*, 4051−4060.

(18) Hong, M.; Lyu, W. Y.; Wang, Y.; Zou, J.; Chen, Z. G. Establishing the Golden Range of Seebeck Coefficient for Maximizing Thermoelectric Performance. *J. Am. Chem. Soc.* **2020**, *142*, 2672−2681.
(19) Zhou, C.; Yu, Y.; Lee, Y.-L.; Ge, B.; Lu, W.; Cojocaru-Miredin, O.; Im, J.; Cho, S.-P.; Wuttig, M.; Shi, Z.; Chung, I. Exceptionally High Average Power Factor and Thermoelectric Figure of Merit in n-type PbSe by the Dual Incorporation of Cu and Te. *J. Am. Chem. Soc.* **2020**, *142*, 15172−15186.
(20) Cao, Y.; Bai, H.; Li, Z.; Zhang, Z. K.; Tang, Y. F.; Su, X. L.; Wu, J. S.; Tang, X. F. Zn-Induced Defect Complexity for the High Thermoelectric Performance of n-type PbTe Compounds. *ACS Appl. Mater. Interfaces* **2021**, *13*, 43134−43143.
(21) Xiao, Y. W.; Wu, Y. X.; Nan, P. F.; Dong, H. L.; Chen, Z. W.; Chen, Z. Q.; Gu, H. K.; Ge, B. H.; Li, W.; Pei, Y. Z. Cu Interstitials Enable Carriers and Dislocations for Thermoelectric Enhancements in n-$PbTe_{0.75}Se_{0.25}$. *Chem* **2020**, *6*, 523−537.
(22) Wang, S. Q.; Yang, Z.; Sun, Y. J.; Xiao, Y.; Zhao, L. D. Synergistically Optimizing Charge and Phonon Transport Properties in n-type PbTe via Introducing Ternary Compound $AgSb(Se, Te)_2$. *J. Alloys Compd.* **2020**, *815*, No. 152463.
(23) Liu, S. X.; Yu, Y.; Wu, D.; Xu, X.; Xie, L.; Chao, X. L.; Bosman, M.; Pennycook, S. J.; Yang, Z. P.; He, J. Q. Coherent Sb/CuTe Core/Shell Nanostructure with Large Strain Contrast Boosting the Thermoelectric Performance of n-type PbTe. *Adv. Funct. Mater.* **2021**, *31*, No. 2007340.
(24) Abdellaoui, L.; Chen, Z. W.; Yu, Y.; Luo, T.; Hanus, R.; Schwarz, T.; Villoro, R. B.; Cojocaru-Miredin, O.; Snyder, G. J.; Raabe, D.; Pei, Y. Z.; Scheu, C.; Zhang, S. Y. Parallel Dislocation Networks and Cottrell Atmospheres Reduce Thermal Conductivity of PbTe Thermoelectrics. *Adv. Funct. Mater.* **2021**, *31*, No. 2101214.
(25) Roychowdhury, S.; Ghosh, T.; Arora, R.; Samanta, M.; Xie, L.; Singh, N. K.; Soni, A.; He, J. Q.; Waghmare, U. V.; Biswas, K. Enhanced Atomic Ordering Leads to High Thermoelectric Performance in $AgSbTe_2$. *Science* **2021**, *371*, 722−727.
(26) Xiang, B.; Liu, J.; Yan, J.; Xia, M.; Zhang, Q.; Chen, L.; Li, J.; Tan, X. Y.; Yan, Q.; Wu, Y. Local Nanostructures Enhanced the Thermoelectric Performance of n-type PbTe. *J. Mater. Chem. A* **2019**, *7*, 18458−18467.
(27) Grossfeld, T.; Sheskin, A.; Gelbstein, Y.; Amouyal, Y. Microstructure Evolution of Ag-Alloyed PbTe-Based Compounds and Implications for Thermoelectric Performance. *Crystals* **2017**, *7*, No. 281.
(28) Wang, H. C.; Bahk, J.-H.; Kang, C.; Hwang, J.; Kim, K.; Kim, J.; Burke, P.; Bowers, J. E.; Gossard, A. C.; Shakouri, A.; Kim, W. Right Sizes of Nano- and Microstructures for High-Performance and Rigid Bulk Thermoelectrics. *Proc. Natl. Acad. Sci. U.S.A.* **2014**, *111*, 10949−10954.
(29) Tan, G. J.; Shi, F. Y.; Hao, S. Q.; Zhao, L. D.; Chi, H.; Zhang, X. M.; Uher, C.; Wolverton, C.; Dravid, V. P.; Kanatzidis, M. G. Non-Equilibrium Processing Leads to Record High Thermoelectric Figure of Merit in PbTe-SrTe. *Nat. Commun.* **2016**, *7*, No. 12167.
(30) Zhao, L. D.; Wu, H. J.; Hao, S. Q.; Wu, C. I.; Zhou, X. Y.; Biswas, K.; He, J. Q.; Hogan, T. P.; Uher, C.; Wolverton, C.; Dravid, V. P.; Kanatzidis, M. G. All-scale Hierarchical Thermoelectrics: MgTe in PbTe Facilitates Valence Band Convergence and Suppresses Bipolar Thermal Transport for High Performance. *Energy Environ. Sci.* **2013**, *6*, 3346−3355.
(31) Zhu, Y.; Hu, L.; Zhan, S.; Ina, T.; Gao, X.; Hong, T.; Zhao, L. D. Breaking the Sodium Solubility Limit for Extraordinary Thermoelectric Performance in p-type PbTe. *Energy Environ. Sci.* **2022**, *15*, 3958−3967.
(32) Wu, H. J.; Zhao, L. D.; Zheng, F. S.; Wu, D.; Pei, Y. L.; Tong, X.; Kanatzidis, M. G.; He, J. Q. Broad Temperature Plateau for Thermoelectric Figure of Merit ZT>2 in Phase-Separated PbTe0.7S0.3. *Nat. Commun.* **2014**, *5*, No. 4515.
(33) Xiao, Y.; Zhao, L. D. Charge and Phonon Transport in PbTe-Based Thermoelectric Materials. *npj Quant. Mater.* **2018**, *3*, No. 55.
(34) Chen, T. T.; Wang, H. C.; Su, W. B.; Mehmood, F.; Wang, T.; Zhai, J. Z.; Wang, X.; Wang, C. L. Low Thermal Conductivity and High Figure of Merit for Rapidly Synthesized n-type $Pb_{1-x}Bi_xTe$ Alloys. *Dalton Trans.* **2018**, *47*, 15957−15966.
(35) Qin, C.; Cheng, L. X.; Xiao, Y. W.; Wen, C. L.; Ge, B. H.; Li, W.; Pei, Y. Z. Substitutions and Dislocations Enabled Extraordinary n-type Thermoelectric PbTe. *Mater. Today Phys.* **2021**, *17*, No. 100355.
(36) Male, J.; Agne, M. T.; Goyal, A.; Anand, S.; Witting, I. T.; Stevanović, V.; Snyder, G. J. The Importance of Phase Equilibrium for Doping Efficiency: Iodine Doped PbTe. *Mater. Horiz.* **2019**, *6*, 1444−1453.
(37) Chang, C.; Wang, D. Y.; He, D. S.; He, W. K.; Zhu, F. Y.; Wang, G. T.; He, J. Q.; Zhao, L. D. Realizing High-Ranged Out-of-Plane ZTs in N-Type SnSe Crystals through Promoting Continuous Phase Transition. *Adv. Energy Mater.* **2019**, *9*, No. 1901334.
(38) Zhou, C. J.; Yu, Y.; Lee, Y. K.; Cojocaru-Miredin, O.; Yoo, B.; Cho, S. P.; Im, J.; Wuttig, M.; Hyeon, T.; Chung, I. High-Performance n-type PbSe-Cu_2Se Thermoelectrics through Conduction Band Engineering and Phonon Softening. *J. Am. Chem. Soc.* **2018**, *140*, 15535−15545.
(39) Xiao, Y.; Zhao, L. D. Seeking New, Highly Effective Thermoelectrics. *Science* **2020**, *367*, 1196−1197.
(40) Pei, Y. Z.; May, A. F.; Snyder, G. J. Self-Tuning the Carrier Concentration of PbTe/Ag_2Te Composites with Excess Ag for High Thermoelectric Performance. *Adv. Energy Mater.* **2011**, *1*, 291−296.
(41) Wang, C.; Zhao, X. D.; Ning, S. T.; Tao, Q. R.; Tang, Y. F.; Chen, Z. Q.; Wu, J. S.; Su, X. L.; Tang, X. F. Phase Boundary Mapping and Suppressing Pb Vacancies for Enhanced Thermoelectric Properties in n-type Sb Doped PbTe Compounds. *Mater. Today Energy* **2022**, *25*, No. 100962.
(42) Chen, S. P.; Wang, Y. C.; Wang, Y. N.; Fan, W. H.; Guo, J. Y.; Chen, J.; Jiang, Y.; Al-Yusufi, R.; Munir, Z. Thermoelectric and Mechanical Characterization of the Utilization of FeTe as an Electrode for Iodine-Doped PbTe. *J. Alloys Compd.* **2022**, *905*, No. 164267.
(43) Zhu, C.; Zhang, J.; Ming, H. W.; Huang, L. L.; Li, Y. Y.; Chen, T.; Li, D.; Zhang, B. L.; Xu, J. T.; Qin, X. Y. Synergistic Optimization of Electrical and Thermal Transport in n-type Bi-Doped PbTe by Introducing Coherent Nanophase $Cu_{1.75}Te$. *J. Materiomics* **2021**, *7*, 146−155.
(44) Wu, H. J.; Chang, C.; Feng, D.; Xiao, Y.; Zhang, X.; Pei, Y. L.; Zheng, L.; Wu, D.; Gong, S. K.; Chen, Y.; He, J. Q.; Kanatzidis, M. G.; Zhao, L. D. Synergistically Optimized Electrical and Thermal Transport Properties of SnTe via Alloying High-Solubility MnTe. *Energy Environ. Sci.* **2015**, *8*, 3298−3312.
(45) Yelgel, Ö. C.; Srivastava, G. P. Thermoelectric Properties of n-type $Bi_2(Te_{0.85}Se_{0.15})_3$ Single Crystals Doped with CuBr and SbI_3. *Phys. Rev. B* **2012**, *85*, No. 125207.
(46) Qian, X.; Wu, H. J.; Wang, D. Y.; Zhang, Y.; Wang, J. F.; Wang, G. T.; Zheng, L.; Pennycook, S. J.; Zhao, L. D. Synergistically Optimizing Interdependent Thermoelectric Parameters of n-type PbSe Through Alloying CdSe. *Energy Environ. Sci.* **2019**, *12*, 1969−1978.
(47) Jia, B. H.; Huang, Y.; Wang, Y.; Zhou, Y. S. Y.; Zhao, X. D.; Ning, S. T.; Xu, X.; Lin, P. J.; Chen, Z. Q.; Jiang, B. B.; He, J. Q. Realizing High Thermoelectric Performance in Non-Nanostructured n-type PbTe. *Energy Environ. Sci.* **2022**, *15*, 1920−1929.
(48) Xiao, Y.; Wu, H. J.; Wang, D. Y.; Niu, C. L.; Pei, Y. L.; Zhang, Y.; Spanopoulos, I.; Witting, I. T.; Li, X.; Pennycook, S. J.; Snyder, G. J.; Kanatzidis, M. G.; Zhao, L. D. Amphoteric Indium Enables Carrier Engineering to Enhance the Power Factor and Thermoelectric Performance in n-type $Ag_nPb_{100}In_nTe_{100+2n}$ (LIST). *Adv. Energy Mater.* **2019**, *9*, No. 1900414.
(49) You, L.; Zhang, J. Y.; Pan, S. S.; Jiang, Y.; Wang, K.; Yang, J.; Pei, Y. Z.; Zhu, Q.; Agne, M. T.; Snyder, G. J.; Ren, Z. F.; Zhang, W. Q.; Luo, J. Realization of Higher Thermoelectric Performance by Dynamic Doping of Copper in n-type PbTe. *Energy Environ. Sci.* **2019**, *12*, 3089−3098.

https://doi.org/10.1021/acs.chemmater.2c03542
Chem. Mater. 2023, 35, 755−763

(50) Luo, Z.-Z.; Zhang, X. M.; Hua, X.; Tan, G. J.; Bailey, T. P.; Xu, J. W.; Uher, C.; Wolverton, C.; Dravid, V. P.; Yan, Q. Y.; Kanatzidis, M. G. High Thermoelectric Performance in Supersaturated Solid Solutions and Nanostructured n-type PbTe-GeTe. *Adv. Funct. Mater.* **2018**, *28*, No. 1801617.
(51) Xiao, Y.; Wu, H. J.; Cui, J.; Wang, D. Y.; Fu, L. W.; Zhang, Y.; Chen, Y.; He, J. Q.; Pennycook, S. J.; Zhao, L. D. Realizing High Performance n-type PbTe by Synergistically Optimizing Effective Mass and Carrier Mobility and Suppressing Bipolar Thermal Conductivity. *Energy Environ. Sci.* **2018**, *11*, 2486−2495.
(52) Su, X. L.; Hao, S. Q.; Bailey, T. P.; Wang, S.; Hadar, I.; Tan, G. J.; Song, T.-B.; Zhang, Q. J.; Uher, C.; Wolverton, C.; Tang, X. F.; Kanatzidis, M. G. Weak Electron Phonon Coupling and Deep Level Impurity for High Thermoelectric Performance $Pb_{1-x}Ga_xTe$. *Adv. Energy Mater.* **2018**, *8*, No. 1800659.

https://doi.org/10.1021/acs.chemmater.2c03542
Chem. Mater. 2023, 35, 755−763